Materials Express

2158-5849/2011/1/144/010
doi:10.1166/mex.2011.1015
www.aspbs.com/mex

Competitive Bonding of Amino and Hydroxyl Groups in Ethanolamine on Si(100)2 × 1: Temperature-Dependent X-Ray Photoemission and Thermal Desorption Studies of Nanochemistry of a Double-Chelating Agent

A. Radi[†] and K. T. Leung[*]

WATLab and Department of Chemistry, University of Waterloo, Waterloo, Ontario, N2L3G1, Canada

Article

Temperature-dependent X-ray photoelectron spectroscopy (XPS) and thermal desorption spectrometry (TDS) have been used to study the room-temperature adsorption and thermal evolution of ethanolamine. Like allylamine, the presence of a broad N 1s feature at 399.1 eV commonly attributed to N–Si indicates N–H dissociative adsorption of ethanolamine, while the O 1s feature at 533.1 eV indicates the formation of Si–O bond and O–H dissociation as found in allyl alcohol. Furthermore, a broad C 1s envelope, corresponding to the C–N feature at 284.9 eV and C–O feature at 285.7 eV, is observed. These XPS data are consistent with the [N, O] bidentate staggered and eclipsed ethanolamine conformer adspecies resulting from N–H dissociation and O–H dissociation, as predicted by our Density Functional Theory (DFT) calculations. The adspecies remains stable upon annealing to 595 K, above which C–N and C–O dissociation occurs, as reflected by the conversion of existing XPS features to a new N 1s feature at 397.7 eV corresponding to Si–N(H)–Si and a new O 1s feature at 532.0 eV corresponding to Si–O–Si, with no loss in the respective total intensities up to 1190 K and 1090 K, respectively. The spectral evolution of the N 1s and O 1s features is also consistent with the emergence of a new C 1s envelop near 285.3 eV, corresponding to the dissociated →C–C← (ethanyl) adspecies, at 595 K. The minor loss (30%) in the total C 1s intensity and the emergence of TDS features of m/z 26, 27, and 28 near 615 K further support that some of the ethanyl adspecies has desorbed as ethylene. The majority of the ethanyl adspecies is found to remain on the surface and is converted at 890 K to SiC, with representative C 1s feature at 283.2 eV. The observed thermal evolution suggests the possibility of thermally controlling the conversion of a double NH and O passivated Si(100) surface at 595 K to a N passivated Si(100) surface at 1190 K. Unlike the multidentate allyl alcohol and allylamine adspecies that are found to be not favoured kinetically, the formation of the present [N, O] bidentate ethanolamine adspecies appears to be kinetically favoured on Si(100)2 × 1.

Keywords: Nanochemistry, Surface Functionalization, Thermal Desorption, Bifunctional Organic Molecules, Dissociative Adsorption, DFT Calculations, XPS, TPD, TDS, Ethanolamine, Si(100)2 × 1.

1. INTRODUCTION

Organic functionalization of a Si(100) surface has attracted a lot of recent attention not just in the semiconductor industry but also in emerging applications, including

[*]Author to whom correspondence should be addressed.
Email: tong@uwaterloo.ca
[†]Present address: Department of Chemistry, University of British Columbia, 2036 Main Mall, Vancouver, British Columbia, V6T 1Z1, Canada.

nanomedicine and molecular electronics.[1–6] These organic adsorbates are essential and versatile in introducing a variety of new functionalities, including optical, electronic, chemical or biological activity and selectivity, on Si surfaces.[3,7,8] In the asymmetric buckled dimer model for the Si(100)2 × 1 surface,[9,10] one of the two dangling bonds of a surface atom combines with one other dangling bond of a neighbouring atom, forming a strong σ bond, while the remaining dangling bonds of the dimer pair in effect produces a weak π bond. The asymmetric charge distribution of the down-atom and the up-atom of the buckled dimer produces an electrophilic-nucleophilic pair, causing remarkably different site-specific reactivity.[9,11] Among the organic molecules commonly used for functionalization, bifunctional molecules are particularly interesting, because one functional group can be used to anchor the molecule to selected sites on the surface, while the other functional group serves as a new reaction site for selective reactions to occur. For example, bifunctional organic molecules have been reported for use as interconnections between two surfaces,[12] and in protein detection,[13] biological nanoprobes,[14] and molecular electronic components.[15]

In order to control the adsorption and the subsequent surface reactions of complex organic molecules on Si(100)2 × 1, systematic studies to better understand the competitions among different functional groups in simpler (or "model") adsorbates would be very useful. We have recently conducted a series of studies involving bifunctional organic molecules on Si(100)2 × 1 surfaces. By comparing the reactivities of several common functional groups, including halogen atoms (Br,[16] Cl),[17] hydroxyl (OH),[18] carbonyl (C=O),[18] carboxylic (COOH),[19] and more recently amino (NH_2) groups,[20] to a reference group such as the ethenyl group (C=C), we obtain insights into factors that control their reactivities on the 2 × 1 dimer surface. In the present work, we give the first inter-comparison between two of these functional groups, particularly, the hydroxyl and amino groups, in a simple bifunctional molecule, ethanolamine ($OH–CH_2–CH_2–NH_2$).[21] Along with allyl alcohol[18] and allylamine,[20] the study of ethanolamine completes the comparison cycle among the OH, NH_2 and C=C groups.[18,20] Ethanolamine is also a nontoxic, biologically interesting molecule that represents one of the basic building blocks of phospholipids in biological membranes, and in addition to the aforementioned nano-applications, it has also been used in industrial scrubbers, power plants, pharmaceutical and household products.[22]

To date, several studies on the interactions of molecules containing either the amino group[23–28] or the hydroxyl group[2,29–33] with the Si(100)2 × 1 surface have been reported. In general, these studies show that the molecules bind to the 2 × 1 surface through either N–H or O–H dissociation, resulting in the formation of Si–N and Si–O bonds, respectively.[2,23–32] In particular, Wu et al.,[23] Cao and Hamers,[24,26,27] Hlil et al.,[25] and Kugler et al.[28] found that different amino-containing molecules (including *tert*-butylamine, diethylamine, and methylethylamine,[23] dimethylamine,[27] 1,4-phenylenediamine[28] and other alkylamines[26]) bind to the 2 × 1 surface through N–H dissociative adsorption by using X-ray photoelectron spectroscopy (XPS). Similarly for the hydroxyl-containing molecules (including propanol,[2] methanol,[29,33] ethanol,[30] isopropanol and *tert*-butanol,[31] 2,3-butanediol[32]), Zhang et al.,[2] Shannon and Campion,[29] Eng et al.,[30] Kim et al.,[31,32] and Casaletto et al.[33] also observed O–H dissociative adsorption on the 2 × 1 surface by using vibrational and electron-based spectroscopic techniques. In addition, a Fourier Transform Infrared and XPS study on the adsorption of formamide (NH_2CHO) on Si(100)2 × 1 reported by Bu and Lin[34] showed that NH_2CHO adsorbs on the 2 × 1 surface through the carboxyl O with the NH_2 group intact.

In our recent work on bifunctional organic molecules, we observe N–H and O–H dissociative adsorption of allylamine and allyl alcohol,[18] respectively. These dissociative adsorption processes are favoured over the [2 + 2] C=C cycloaddition, which indicates that the NH_2 and OH groups are more reactive than the ethenyl group on the 2 × 1 surface. The present work will provide the first data on the adsorption of ethanolamine on Si(100)2 × 1, comparing the reactivities of the NH_2 and OH groups specifically within a single molecule. Using XPS and thermal desorption spectrometry (TDS), we show that the adsorption of ethanolamine involves dissociation of both the N–H and O–H bonds on the 2 × 1 surface, producing a unique bridge-like structure [–O→C–C←N(H)–] between two Si dimer atoms. This result suggests that the NH_2 and OH groups are equally reactive on the Si dimer sites. Our temperature-dependent XPS spectra and TDS profiles further reveal the remarkable stabilities of the resulting organized nanoscale templates of NH and O terminated Si dimer pairs, with ethylene as the only desorbate. These observations are supported by our Density Functional Theory (DFT) calculations of the relevant adstructures on a double-dimer model surface of a $Si_{15}H_{16}$ cluster.

2. EXPERIMENTAL AND COMPUTATIONAL DETAILS

A home-built ultrahigh vacuum dual-chamber system with base pressure better than 1×10^{-10} Torr used for the present work has been described in detail in our earlier work.[35] Briefly, the upper sample preparation chamber was equipped with an ion-sputtering gun for sample cleaning, a four-grid retarding field optics for characterization of surface morphology by low energy electron diffraction and of surface cleanliness by Auger electron spectroscopy, and a gas handling system for sample dosing.

The lower analysis chamber was equipped with facilities for XPS and TDS analysis. An XPS electron spectrometer (VG Scientific CLAM-2), consisting of a hemispherical analyser of 100 mm mean radius and a triple-channeltron detector, was used to analyse photoelectrons excited by unmonochromatic Al K_α radiation (at 1486.6 eV photon energy) delivered by a twin-anode X-ray source. A differentially pumped 1–300 amu quadrupole mass spectrometer (VG Quadrupole SXP Elite) was employed to obtain TDS profiles of selected mass fragments from the sample, at a linear heating rate of 2 K s^{-1} provided by a home-built programmable proportional–integral–differential temperature controller.[19]

The Si sample (10×14 mm^2 in size) was cut from a single-side polished, *p*-type (B-doped) Si(100) wafer (0.4 mm thick) with a resistivity of 0.0080–0.0095 Ω cm (Virginia Semiconductors). After solvent-cleaned and hydrogen-terminated by using a standard RCA method under ambient condition,[36] the sample was mounted on the sample manipulator mechanically by using Ta clamps at both ends, with a type-*K* thermocouple (wrapped in a Ta foil) securely fastened onto the front face at one end of the sample.[19, 37] The surface was cleaned in the preparation chamber by repeated cycles of Ar ion sputtering for 30 minutes (at an Ar gas pressure of 4×10^{-5} Torr, 20 mA emission current, and 1.5–2 keV ion beam energy) followed by annealing to 900 K for 5 minutes by passing a direct current through the sample. The sample was then flash-annealed to 1100 K for 20 s to obtain the 2×1 reconstructed surface. The cleanliness of the surface was verified by the sharpness of the low energy electron diffraction patterns and the lack of contaminant XPS features (e.g., C 1s and O 1s).

Ethanolamine (99.9% purity), a colourless liquid, was purchased from Sigma-Aldrich and was degassed by several freeze-pump-thaw cycles. Ethanolamine was exposed to the clean Si(100)2×1 surface by backfilling the sample preparation chamber to an appropriate exposure pressure (typically 1×10^{-6} Torr, as monitored by an uncalibrated ionization gauge) using a variable leak valve for a preselected time duration. All exposures were performed at room temperature and reported in units of Langmuir (1 L = 1×10^{-6} Torr s). Unless stated otherwise, a saturation exposure has been used for both temperature-dependent XPS and TDS experiments. XPS spectra were obtained with an acceptance angle of ±4° at normal emission from the Si sample and a constant pass energy of 50 eV, giving an effective energy resolution of 1.4 eV full-width-at-half-maximum (FWHM) for the Si 2p photopeak. The binding energy (BE) scale of the XPS spectra has been calibrated to the Si 2p feature of the bulk at 99.3 eV.[16] After appropriate background subtraction (using the Shirley background), individual XPS spectral components can be fitted with Gaussian–Lorentzian lineshapes by using the CasaXPS software. For temperature-dependent XPS experiments, the sample was flash-annealed to the preselected temperature and allowed to cool back to room temperature before collecting the XPS spectra. To ensure that the detected mass fragments originate only from the Si sample, TDS profiles were collected after carefully positioning the sample at 1 mm from the orifice (2 mm dia.) of the differentially pumped housing of the mass spectrometer.[37] The temperature scale has been calibrated by using the temperature of desorption maximum for recombinative H_2 desorption from Si monohydrides (780 K),[38] and the uncertainty of determining the desorption maxima was estimated to be ± 30 K.

Equilibrium structures, total energies and vibrational wavenumbers of respective bonds were calculated by using the DFT/B3LYP method[39] with the Gaussian 03 package.[40] The widely used hybrid B3LYP functional,[18–20] consisting of Becke's 3-parameter gradient-corrected exchange functional[41] and the Lee-Yang-Parr correlation functional,[42] has been employed for determining the ethanolamine adsorption structures on Si(100)2×1. Four moderately sized basis sets, including 6-31G(d), 6-31+G(d), 6–31++G(d), and 6–31++G(d, p), were used and found to give similar optimized geometries, with the larger basis set providing a lower total energy. To model the Si(100)2×1 surface, we employed the double-dimer cluster ($Si_{15}H_{16}$)[10, 43, 44] created by using a new procedure discussed elsewhere.[20, 45]

In accord with the earlier experimental and theoretical studies,[46–49] our DFT calculations have reaffirmed that the gauche structure is the most stable geometry for ethanolamine in the gas phase. The possibility of the conversion between the gas-phase structures induced by the surface, which may lead to a distribution of several products on the Si(100)2×1 surface, has prompted us to consider both gauche (eclipsed) and trans (staggered) conformers in our calculations. Following the work of Vorobyov et al.,[49] we obtained the equilibrium structures for the free eclipsed ethanolamine as the most likely conformer for free ethanolamine. Another less likely equilibrium structure was also considered (the staggered conformer), in order to take into account the possible surface effect in transforming the eclipsed to staggered structure and vice versa as the molecule approaching the surface.

The optimized conformer structures were then combined with that of the $Si_{15}H_{16}$ cluster to construct the adsorbate-substrate configurations (ASCs). The corresponding adsorption energy, ΔE, was estimated by the difference between the total energy for the optimized structures of the ASCs and the sum of the total energies of a free conformer and of the $Si_{15}H_{16}$ cluster. Frequency calculation was also performed for all of the optimized geometries, in order to assure that the local minima correspond to the equilibrium structures and not transition-state structures. All the total energies were obtained without zero-point correction and no basis set superposition error correction was made to ΔE.

3. RESULTS AND DISCUSSION

3.1. DFT Computational Study of Adsorbate-Substrate Configurations

Figure 1 shows the optimized free-molecule geometries of two ethanolamine conformers at 6-31++G(d, p) basis set. Based on the calculated total energies and vibrational wavenumbers, we identify two local minima at dihedral angles of 55.4° and 177.8°. Table I compares the total energies for the optimized geometries of the conformers for four different basis sets. The total energies of the conformers are found to be effectively identical within the limitation of the present calculation, i.e., with a difference less than 0.005 hartree or 13.05 kJ mol^{-1}.

Figure 2 shows three different types of plausible ASCs obtained from geometry optimization of ethanolamine eclipsed (E) conformer (Fig. 1, Structure A) and staggered (S) conformer (Fig. 1, Structure B) on a double-dimer $Si_{15}H_{16}$ model surface for Si(100)2 × 1. In particular, single dissociation of the O–H or N–H bond leads to unidentate ASCs through the respective formation of the Si–O and Si–H bonds (Figs. 2(a, c)) or Si–N and Si–H bonds on a Si dimer pair (Figs. 2(b, d)). Dissociation of both the O–H and N–H bonds could give rise to the corresponding bidentate ASCs (Figs. 2(e–g)). Table I summarizes the corresponding adsorption energies and total energies for the ASCs calculated by the DFT/B3LYP method for four different basis sets. Not surprisingly, the total energies of the ASCs obtained by the larger basis sets are more negative than those obtained by the smaller basis sets. The adsorption energies, on the other hand, appear to generally follow an opposite trend with increasing size of the basis set, i.e., with the 6-31++G(d, p) basis set providing the least negative value. Evidently, the adsorption energies for unidentate O–H dissociation ASCs E1 (S1) [−319.95 kJ mol^{-1} (−254.76 kJ mol^{-1})] are found to be more negative than the corresponding unidentate N–H dissociation ASCs E2 (S2) [−210.72 kJ mol^{-1} (−216.99 kJ mol^{-1})] (Fig. 2), which suggests that O–H dissociation is more thermodynamically favourable than N–H dissociation.

In the case of [O, N] bidentate ASCs, concurrent O–H and N–H dissociation of both the eclipsed and staggered conformers leads to the most thermodynamically stable adstructures with discernibly similar adsorption energies and a slight difference in the molecule geometry on the surface. The intra-dimer [O, N] bidentate ASCs (ΔE = (−435.23)–(−448.26) kJ mol^{-1}, Fig. 2(e)) are only slightly more stable than the corresponding inter-dimer ASCs (ΔE = (−431.29)–(−447.80) kJ mol^{-1}, Fig. 2(f)), while the cross-dimer ASCs give the least negative ΔE_s ((−373.66)–(−410.47) kJ mol^{-1}, Fig. 2(g)). It is of interest to note that the intra-dimer [O, N] bidentate ASC (Fig. 2(e)) forms a six-member organosilicon ring [Si–O→C–C←N(H)–Si], while the inter-dimer ASC (Fig. 2(f)) and cross-dimer ASC (Fig. 2(g)) represent a seven-member and a eight-member rings, respectively. In organic chemistry, the reaction pathway is generally faster for closing a six-member ring complex than a seven-member or eight-member ring complex,[50] which suggests that the formation of the intra-dimer ASCs would be faster, i.e., kinetically more favorable, than the inter-dimer ASCs and cross-dimer ASCs. As we shall show below that these bidentate ethanolamine ASCs, unlike their corresponding multidentate allyl alcohol[18] and allylamine counterparts,[20] appear to be the most likely adstructures with respect to the experimental data.

It is also of interest to note that the bond lengths for the unidentate and bidentate O–H dissociation and N–H dissociation ASCs are found to be essentially unchanged (within 0.01 Å) from those of the free conformers. The Si–O (1.69 Å) and Si–N bond lengths (1.75 Å) are also identical for all the unidentate and bidentate ASCs. The most notable structural change is found in the dihedral angle of unidentate O–H dissociation ASC E1 (114.9°) from that of the free E conformer (55.4°). On the other hand, the dihedral angles for the other three unidentate ASCs (E2, S1 and S2) are relatively unchanged from those of the corresponding free E and S conformers. Changes in the dihedral angles for bidentate ASCs (74.5° for E3, 97.1° for E4, and 59.9° for E5) are considerably less pronounced with respect to the free E conformer (55.4°) than the S conformer (177.8°).

3.2. XPS Study of Ethanolamine Adsorption on Si(100)2 × 1 at Room Temperature

The XPS spectra of ethanolamine on Si(100)2 × 1 have been obtained for a number of room-temperature exposures (0.5 L, 2.5 L, 5 L, 10 L, 20 L, 50 L, 100 L, and

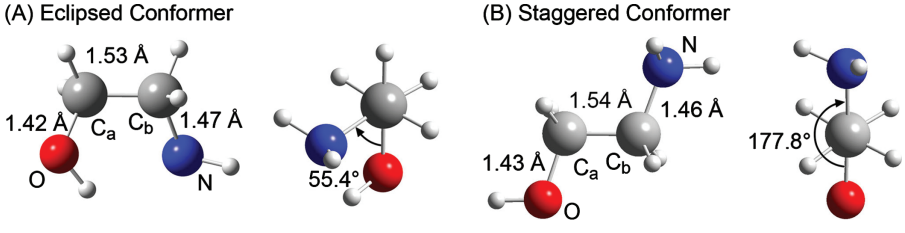

Fig. 1. The equilibrium structures of the (A) eclipsed and (B) staggered conformers of ethanolamine obtained by DFT/B3LYP/6-31++G(d, p) calculation.

Article

Table I. Adsorption energies (in kJ mol^{-1}), where applicable, and total energies (in hartree), given in square parentheses, of the double-dimer $Si_{15}H_{16}$ cluster, free ethanolamine eclipsed (E) and staggered (S) conformers, and different adsorbate-substrate configurations (ASCs) obtained by DFT/B3LYP calculations with different basis sets.

Adsorption energy (kJ mol^{-1}) [Total energy (hartree)]		Basis set			
		6-31G(d)	6-31+G(d)	6-31++G(d)	6-31++G(d, p)
$Si_{15}H_{16}$ cluster[20]		[−4352.059071]	[−4352.071932]	[−4352.073387]	[−4352.091204]
Ethanolamine conformers with	55.4° (E)	[−210.3795811]	[−210.3956644]	[−210.3959650]	[−210.4132174]
Dihedral angle	177.8° (S)	[−210.3741313]	[−210.3904263]	[−210.3908023]	[−210.4082450]
ASC E1		−357.12 [−4562.574671]	−333.93 [−4562.594783]	−334.06 [−4562.596590]	−319.95 [−4562.626283]
ASC E2		−222.04 [−4562.523222]	−215.21 [−4562.549567]	−215.35 [−4562.551374]	−210.72 [−4562.584680]
ASC S1		−280.72 [−4562.540123]	−266.89 [−4562.564011]	−264.80 [−4562.565047]	−254.76 [−4562.596481]
ASC S2		−228.08 [−4562.520071]	−222.01 [−4562.546917]	−219.35 [−4562.547734]	−216.99 [−4562.582095]
ASC E3		−472.34 [−4562.618558]	−452.21 [−4562.639833]	−451.91 [−4562.641476]	−435.23 [−4562.670191]
ASC E4		−467.75 [−4562.616807]	−447.63 [−4562.638090]	−447.71 [−4562.639874]	−431.29 [−4562.668690]
ASC E5		−412.09 [−4562.595610]	−389.85 [−4562.616081]	−389.80 [−4562.617819]	−373.66 [−4562.646739]
ASC S3		−486.64 [−4562.618554]	−465.96 [−4562.639831]	−465.46 [−4562.641475]	−448.26 [−4562.670181]
ASC S4		−487.25 [−4562.618786]	−464.99 [−4562.639464]	−464.79 [−4562.641218]	−447.80 [−4562.670004]
ASC S5		−451.24 [−4562.605071]	−427.59 [−4562.625218]	−427.22 [−4562.626907]	−410.47 [−4562.655787]

200 L). No discernible difference in the profile shape is found, which indicates that the adspecies are the same over the studied exposure range. Figure 3 shows representative O 1s, N 1s and C 1s spectra for a low (5 L) and a saturation exposures (100 L). Evidently, except for the lower overall intensities, the shapes of the O 1s, N 1s and C 1s spectra are essentially unchanged from the low exposure to the saturation exposure. Based on the reported literature values for N 1s BEs for the N–H dissociation adspecies (398.5–399.1 eV),[23–28] –NH_2 physisorbed (399.5–400.1 eV) and N dative-bonded species (401.1–402.3 eV),[23–28] all on Si(100)2 × 1 surfaces, the single N 1s feature observed at 399.1 eV BE (with 1.6 eV FWHM) (Figs. 3(c, d)) can be assigned to Si–N(H)–C←. The present N 1s assignment is also in excellent agreement with the N 1s BEs for allylamine on Si(100)2 × 1 (398.9 eV)[20] and glycine on Si(111)7 × 7 (399.1 eV),[51] for which dissociative N–H adsorption has been demonstrated. The lower N 1s BE with respect to the terminal amino group commonly found at 399.5–402.3 eV BE[23–28] can therefore be used to rule out the presence of adspecies not involving N–H dissociation on the surface, i.e., unidentate O–H dissociation ASCs E1 and S1 (Fig. 2). Furthermore, a single, broad O 1s peak (with 1.9 eV FWHM) is observed at 533.1 eV (Figs. 3(a, b)), which is in good accord with the Si–O–C← moiety found for allyl alcohol and allyl aldehyde (532.6–532.7 eV)[18] and formamide (533.4 eV)[34] adspecies on Si(100)2 × 1. The O 1s feature therefore suggests the presence of O–H dissociation adspecies and the formation of Si–O bonds, which excludes the N–H dissociation unidentate ACSs: E2 and S2 (Fig. 2). In addition, the broad C 1s spectra (Figs. 3(e, f)) can be fitted with two peaks at 284.8 eV and 285.7 eV BE (with 2.2 eV FWHM), which can be attributed to C_b–N and C_a–O bonds, respectively, with an expected unity stoichiometric ratio. The observed higher BEs can be used to rule out the presence of Si−C bonds, with BEs commonly found at 283.2–284.3 eV.[24, 26, 27] However, the observed BEs are somewhat lower than those reported in the literature for adspecies with individual –C–N–Si (286.0–286.2 eV)[24, 26, 27] and –C–O–Si components (285.4–286.9 eV),[18, 32, 52] which is likely due to the formation of a six-member ring found in the bidentate ASCs E3 and S3, as discussed further below. The assertion of the [O, N] bidentate ASCs as the only plausible ethanolamine adstructures on Si(100)2 × 1 can be supported by considering the spectral evolution as a function of temperature discussed below.

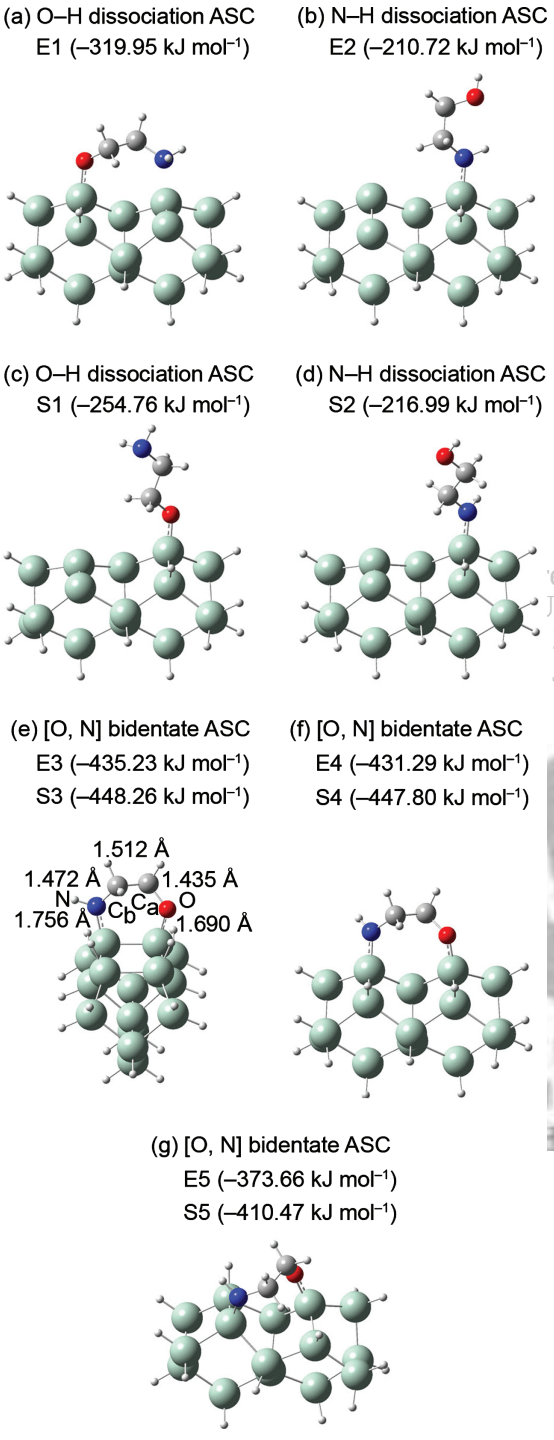

Fig. 2. Optimized geometries of the adsorbate-substrate configurations (ASCs) for eclipsed (a, b) and staggered conformers (c, d) of ethanolamine on a model Si(100)2 × 1 surface: (a, c) O–H dissociation, (b, d) N–H dissociation, and (e) intra-dimer, (f) inter-dimer, and (g) cross-dimer [O, N] bidentate products. The corresponding adsorption energies calculated with the 6-31++G(d, p) basis set are given in parentheses.

3.3. Temperature-Dependent XPS and TDS Studies of Thermal Evolution Products

XPS spectra of N 1s, C 1s and O 1s regions for a saturation (100 L) exposure of ethanolamine on Si(100)2 × 1 collected upon flash-annealing to different temperatures are shown in Figure 4. The corresponding intensities of individual fitted components, relative to the intensity of the Si 2p peak, are also shown as a function of flash-annealing temperature. Up to the flash-annealing temperature of 595 K, the N 1s feature for Si–N(H)–C← at 399.1 eV is found to be essentially unchanged in both intensity and spectral shape (Fig. 4(c)). From 695 K to 890 K, the N 1s feature for Si–N(H)–C← has diminished completely, while a new feature at 397.7 eV BE emerges and becomes the dominant feature. The intensity of the latter feature remains effectively the same upon further flash-annealing to 1190 K. In accord with the N 1s BE for amino-containing molecules (397.2–397.8 eV) on Si(100) reported earlier,[23–28] the N 1s feature at 397.7 eV can be assigned to Si–NH, present either as a radical or bridge-bonded to a second Si atom as Si–N(H)–Si, resulting from C–N bond cleavage. The overall intensity of N 1s feature remains effectively unchanged up to the highest flash-annealing temperature (Fig. 4(d)), which indicates predominant dissociative conversion of the Si–N(H)–C← moiety to Si–NH species (at 695–890 K) on the surface without any relevant N-containing desorbates, as shown by our TDS data below.

The O 1s spectrum (Fig. 4(a)) appears to follow similar thermal evolution as the N 1s spectrum (Fig 4(c)). In particular, the O 1s peak at 533.1 eV remains stable in intensity and peak profile up to a flash-annealing temperature of 595 K, and it becomes totally diminished at 890 K while a new emerging feature at 532.0 eV, commonly assigned to Si–O–Si,[18, 34] grows in intensity. The intensity of the latter feature remains essentially unchanged up to 1090 K and becomes totally quenched at 1190 K (Fig. 4(b)), likely due to diffusion of O into the bulk. Given that the bond dissociation energy follows the order: C–N (356 kJ mol^{-1}) < C–C (385 kJ mol^{-1}) < C–O (395 kJ mol^{-1}),[53] the appearance of Si–O–Si feature at 532.0 eV also marks the on-set of total fragmentation of the adspecies.

Unlike the N 1s and O 1s spectra, the thermal evolution of the corresponding C 1s spectral envelope is more complex. In particular, the C 1s band containing the C_b–N and C_a–O features (at 284.8 eV and 285.7 eV respectively) remains unchanged up to the flash-annealing temperature of 595 K (Fig. 4(e)), above which a discernible reduction in intensity is found. Between 595 K and 795 K (Fig. 4(e)), the intensity of the C 1s band undergoes major reduction in intensity and diminishes completely at 995 K. A new feature at 284.2 eV corresponding to C–C[54, 55] emerges at 695 K and remains unchanged in intensity up to 890 K, above which its intensity becomes completely reduced (at 995 K). At 795 K, the SiC feature at 283.2 eV[19, 23–26] emerges and grows in intensity, becoming the dominant C 1s feature up to 1190 K. The 30% loss of total C 1s intensity at 595–795 K indicates desorption of C-containing fragments (likely ethylene as shown in our TDS data

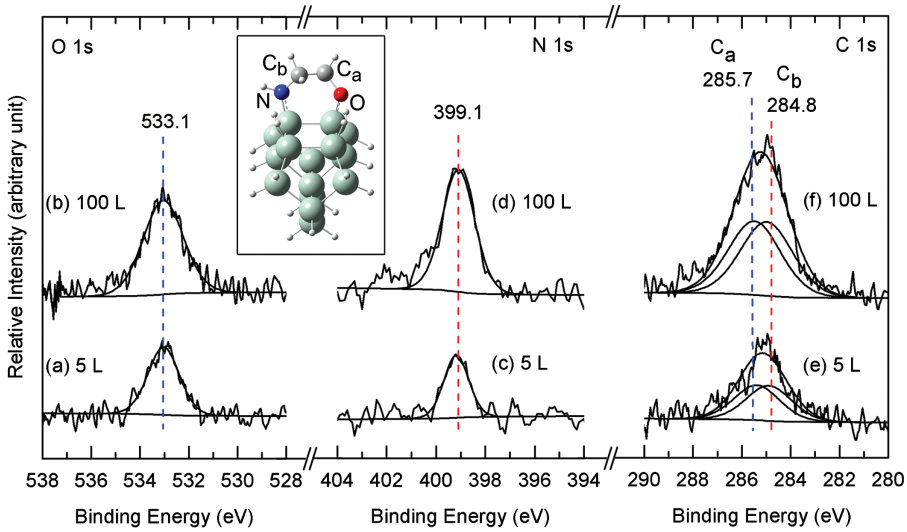

Fig. 3. XPS spectra of O 1s (right), N 1s (center) and C 1s regions (left) for (a, c, e) a low (5 L) and (b, d, f) a saturation (100 L) exposures of ethanolamine on Si(100)2 × 1 at room temperature. The inset shows a plausible [O,N] bidentate adstructure with the methylene C atoms bonded to O (C_a) and N (C_b) appropriately identified.

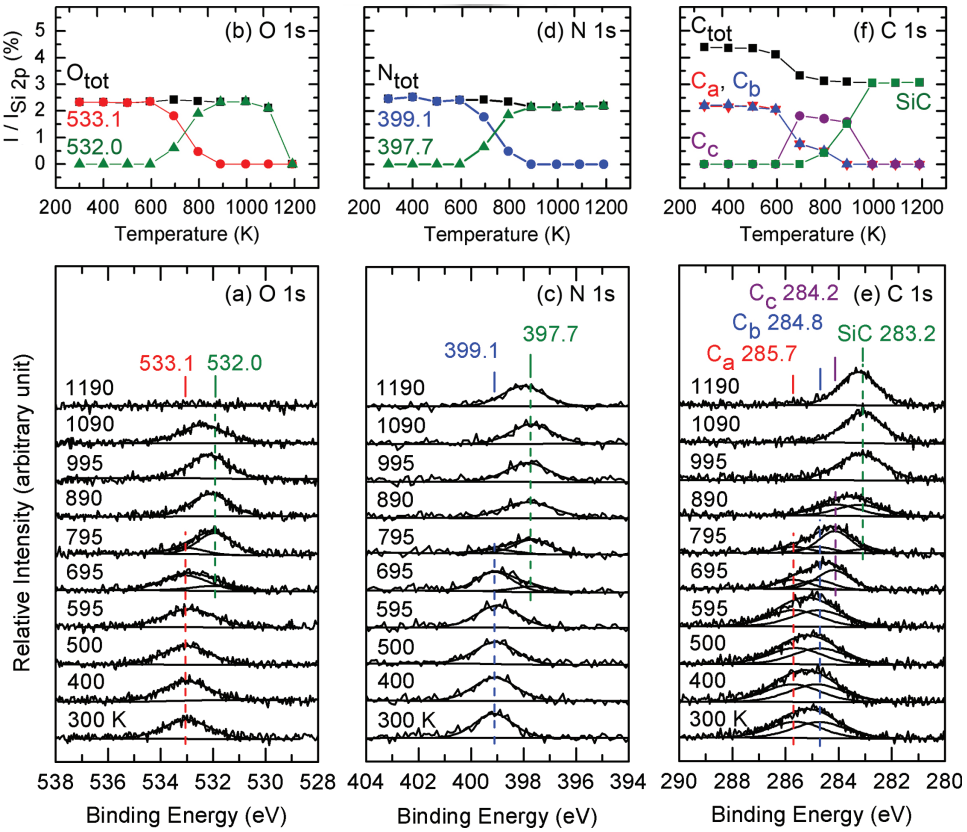

Fig. 4. Temperature-dependent XPS spectra of (a) O 1s, (c) N 1s and (e) C 1s regions for a saturated exposure (100 L) of ethanolamine on Si(100)2 × 1 at room temperature, and upon sequential flash-annealing to 400 K, 500 K, 595 K, 695 K, 795 K, 890 K, 995 K, 1090 K and 1190 K. Corresponding temperature profiles of the intensities of (b) O 1s (I_{O1s}), (d) N 1s (I_{N1s}) and (f) C 1s (I_{C1s}) for Si–O–C← at 533.1 eV, Si–O–Si at 532.0 eV, Si–N(H)–C← at 399.1 eV, Si–N(H) at 397.7 eV, C_a at 285.7 eV, C_b at 284.8 eV, C_c at 284.2 eV, and SiC at 283.2 eV, along with their total intensities O 1s (O_{tot}), N 1s (N_{tot}) and C 1s (C_{tot}), all with respect to Si 2p ($I_{Si\ 2p}$).

Article

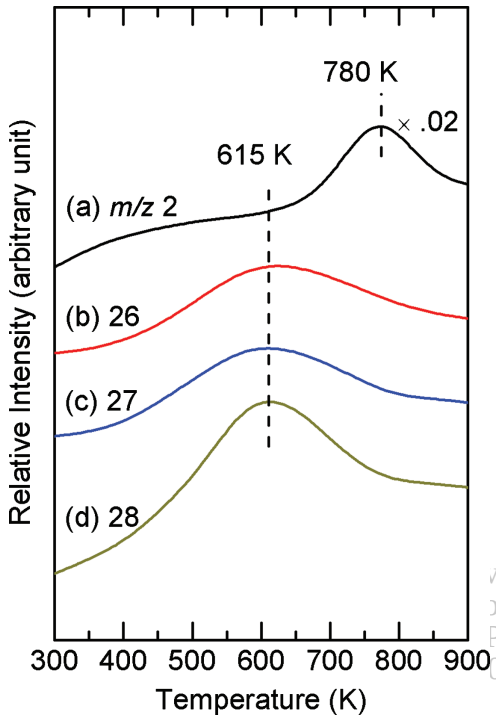

Fig. 5. TDS profiles for selected mass fragments of m/z (a) 2, (b) 26, (c) 27, and (d) 28 for a saturation (100 L) exposure of ethanolamine on Si(100)2 × 1 at room temperature.

below). At 795 K, the remaining adspecies undergoes further dissociation likely first into C–C containing fragments and CH_2 fragments, followed by formation of SiC.

To determine the desorption products thermally evolved from the adspecies remaining on the surface (as probed by the temperature-dependent XPS spectra in Fig. 4), TDS experiments were performed. Figure 5 shows the TDS profiles, after smoothing the curves with adjacent point averaging, of selected mass fragments of m/z 2, 26, 27, and 28 for a room-temperature saturation exposure (100 L) of ethanolamine on Si(100)2 × 1. It should be noted that we have also monitored but found no detectable intensity for other N-containing mass fragments, including m/z 17 (NH_3^+) and 30 ($CH_2NH_2^+$), corresponding to the parent mass of ammonia and to the base masses of ethanolamine and other fragments such as ethylamine and methylamine, respectively.[21] The lack of TDS signals from these fragments indicates that no N-containing species desorbs from the surface and that the N surface content is preserved. This result is in excellent accord with the effective constant total N 1s XPS intensity found up to the maximum flash-annealing temperature (1190 K) shown in Figure 4(d), which confirms that the ethanolamine adspecies (with the N 1s feature at 399.1 eV BE) predominantly converts to Si–N(H)–Si (with N 1s feature at 397.7 eV BE) upon annealing (above 595 K). We also do not detect any TDS signals for m/z 31 (CH_2OH^+), which represents the O-containing mass fragments from ethanol and methyl alcohol.[21] The lack of any detectable TDS signals from O-containing fragments indicates O-containing species, like N-containing species, do not desorb from the surface up to the maximum desorption temperature used in the experiment (1190 K). This result is also in excellent agreement with the total O 1s XPS signal remaining unchanged up to 1090 K (Fig. 4(b)), above which O diffusion into the bulk occurs. Finally, the lack of TDS signals for m/z 29 and m/z 30 ($C_2H_6^+$), and m/z 25 (C_2H^+) can be used to exclude the formation of ethane and acetylene, respectively.[21]

Of the mass fragments that we obtain TDS profiles, the large desorption feature for m/z 2 observed at 780 K (Fig. 5(a)) can be attributed to the recombinative desorption of H_2 from silicon monohydrides.[38] The remaining TDS feature for m/z 28, along with those TDS peaks for

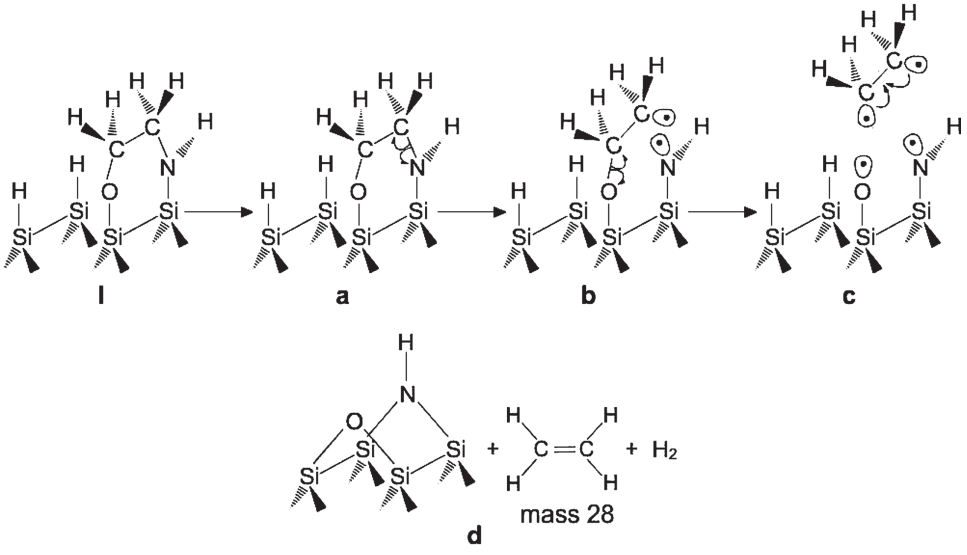

Fig. 6. Schematic model for thermal evolution of an intra-dimer [O, N] bidentate adsorbate-substrate configuration, depicting a possible pathway for the formation of ethylene and H_2 as desorption products, along with Si–N(H)–Si and Si–O–Si as the surface species.

m/z 27 and m/z 26 at approximately half of its intensity (all with desorption maxima at 615 K), corresponds to molecular desorption of ethylene, in excellent accord with the relative intensities of m/z 28 ($C_2H_4^+$, parent and base mass), m/z 27 ($C_2H_3^+$) and m/z 26 ($C_2H_2^+$) found in the cracking pattern of ethylene.[21] The desorption of ethylene therefore corresponds to the observed loss of C 1s intensities at 284.8 eV and 285.7 eV BE between 595 K and 695 K shown in Figure 4(f), which in turn confirms our hypothesis that part of the adspecies desorbs as ethylene.

The formation of ethylene can be easily envisioned from the intra-dimer [O, N] bidentate ASC (Fig. 2(e)) in a schematic pathway shown in Figure 6. In this model, the intra-dimer [O, N] bidentate ASC first undergoes a C–N bond cleavage to form Si–O–CH_2–CH_2• and Si–N(H)• radicals (Step a). The resulting Si–O–CH_2–CH_2• radical then undergoes a C–O bond cleavage, producing two other radicals, Si–O• and •CH_2–CH_2• (Step b), the latter of which becomes molecular ethylene CH_2=CH_2 (Step c). The remaining Si–N(H)• and Si–O• species further react with a neighbouring Si atom, forming Si–N(H)–Si and Si–O–Si, while the Si monohydrides recombine to produce H_2 (Step d).

4. CONCLUDING REMARKS

In the present work, we have carried out temperature-dependent XPS and TDS experiments on the room-temperature adsorption of ethanolamine on Si(100)2 × 1. Detailed DFT calculations, involving both the eclipsed and staggered conformers of ethanolamine on a model surface based on the double-dimer $Si_{15}H_{16}$ cluster, have also been employed to interpret our data. Our XPS data show that room-temperature adsorption of ethanolamine on Si(100)2 × 1 leads to a [O, N] bidentate adspecies, instead of the unidentate adspecies involving single N–H or O–H dissociation. This result is in good accord with the previous work on the adsorption of amino-containing and hydroxyl-containing molecules on Si(100), in which N–H dissociative adsorption through the amino group[23–28] and O–H dissociative adsorption through the hydroxyl group are found to be the primary processes, respectively.[2, 29–33] In our earlier work on amino-containing molecule (allylamine),[20] we showed that the adsorption occurs by the cleavage of the N–H bond and the formation of Si–N bond. For O-containing molecules (allyl alcohol, allyl aldehyde,[18] acetic acid,[56] and acrylic acid and propanic acids)[19] on Si(100)2 × 1, we demonstrated that adsorption proceeds through surface reactions of the hydroxyl,[18] carbonyl,[18] and carboxyl[19] groups, by forming O–Si bonds, with the ethenyl group remaining intact. The present work also shows that both the amino and the hydroxyl group react with the 2 × 1 surface through double N–H and O–H dissociation, respectively, forming N–Si and O–Si on the surface. The geometry of the molecule, involving especially the two ethanyl carbon atoms, enables the molecule to rearrange on the surface and bind through both of its ends forming a bridge of Si–O→C–C← N(H)–Si. Our DFT calculations based on the double-dimer $Si_{15}H_{16}$ cluster model surface also support the [O, N] bidentate adspecies as the preferred adstructures with adsorption energies of (−381.22)–(−448.87) kJ mol^{-1}, with the intra-dimer [O, N] bidentate with six-member ring complex [Si–O→C–C← N(H)–Si] being the most stable. The formation of a six-membered ring structure is in marked contrast to that found for formamide, which binds to the surface by forming Si–O bond, leaving the NH_2 group intact.[34] This difference could be attributed to the overall length of the respective adspecies. The formation of ethylene as the sole desorption product and the absence of N– or O-containing species up to temperature of 1190 K indicate the stability of the adsorbate on the surface, particularly the Si–N and the Si–O species.

The formation of Si–N(H), Si–N and Si–O above 595 K is also confirmed by the presence of the respective N 1s and O 1s features in our temperature-dependent XPS study. Surface functionalization of Si(100)2 × 1 by ethanolamine therefore offers a number of interesting control opportunities, by first converting the "double-bond" of a Si dimer of the 2 × 1 surface to a C–C bond of the "bridge" structure, creating a stable, passivated surface. The study of the competition between the adsorption of the hydroxyl and amino groups reveals that both are likely to occur on the surface. By annealing the functionalized hydrophobic surface to 890 K, the organic moiety is desorbed and the surface is transformed to a unique N– and O-terminated Si (with the atoms likely interchanged in their positions in a periodic fashion). This in effect converts the hydrophobic saturated-hydrocarbon surface [Si–O→C–C←N(H)–Si] to a hydrophilic oxygen (Si–O) and nitrogen (Si–N) mixed surface. Such a conversion can be easily achieved by controlling the annealing temperature and can play an important role in developing the intriguing reaction pathways for organic nanochemistry on a Si substrate.

Acknowledgment: This work was supported by the natural sciences and engineering research council of canada. The calculations were performed in part at the WHALE cluster of the Shared Hierarchical Academic Research Computing Network supported by the governments of Canada and the province of Ontario. We are grateful to Dr. Maryam Ebrahimi for helpful discussion of various relevant aspects of surface chemistry.

References and Notes

1. S. Carniato, J.-J. Gallet, F. Rochet, G. Dufour, and F. Bournel, *Phys. Rev. B* 76, 085321 (**2007**).
2. L. Zhang, A. J. Carmen, and S. M. Casey, *J. Phys. Chem. B* 107, 8424 (**2003**).
3. S. F. Bent, *J. Phys. Chem. B* 106, 2830 (**2006**).

4. N. Sheppard, *Ann. Rev. Phys. Chem.* 39, 589 (**1988**).
5. S. M. Barlow and R. Raval, *Surf. Sci. Rep.* 50, 201 (**2003**).
6. Z. Ma and F. Zaera, *Surf. Sci. Rep.* 61, 229 (**2006**).
7. X. Wang, R. Q. Zhang, T. A. Niehaus, and T. Frauenheim, *J. Phys. Chem. C* 111, 2394 (**2007**).
8. Z. Zhu, A. Srivastava, and R. M. Osgood, Jr., *J. Phys. Chem. B* 107, 13939 (**2003**).
9. J. Yoshinobu, *Prog. Surf. Sci.* 77, 37 (**2004**).
10. J. Li, Y.-Q. Qu, K.-L. Han, and G.-Z. He, *Surf. Sci.* 586, 45 (**2005**).
11. C. B. Duke, *Chem. Rev.* 96, 1237 (**1996**).
12. J. Zhu, M. Yudasaka, M. Zhang, D. Kasuya, and S. Iijima, *Nano Lett.* 3, 9 (**2003**).
13. M. Voue, E. Goormaghtigh, F. Homble, J. Marchand-Brynaert, J. Conti, S. Devouge, and J. De Coninck, *Langmuir* 23, 949 (**2007**).
14. O. Veiseh, C. Sun, J. Gunn, N. Kohler, P. Gabikian, D. Lee, N. Bhattarai, R. Ellenbogen, R. Sze, A. Hallahan, J. Olson, and M. Zhang, *Nano Lett.* 5, 6 (**2005**).
15. H. Haick and D. Cahen, *Acc. Chem. Res.* 41, 359 (**2008**).
16. X. J. Zhou, Q. Li, Z. H. He, X. Yang, and K. T. Leung, *Surf. Sci.* 543, L668 (**2003**).
17. X. J. Zhou and K. T. Leung, *Surf. Sci.* 600, 468 (**2006**).
18. M. Ebrahimi and K. T. Leung, *Surf. Sci.* 603, 1203 (**2009**).
19. M. Ebrahimi, J. M. Chong, and K. T. Leung, *J. Phys. Chem. C* 114, 2947 (**2010**).
20. A. Radi, M. Ebrahimi, and K. T. Leung, *Surf. Sci.* 604, 1073 (**2010**).
21. S. E. Stein, NIST Mass Spec Data Center, Mass Spectra, NIST Chemistry Webbook, NIST Standard Reference Database Number 69, edited by P. J. Linstrom and W. G. Mallard, National Institute of Standards and Technology, Gaithersburg, June (**2005**), http://webbook.nist.gov.
22. C. Reinemann, R. Stoltenburg, and B. Strehlitz, *Anal. Chem.* 81, 3973 (**2009**).
23. J. B. Wu, Y. W. Yang, Y. F. Lin, and H. T. Chiu, *J. Phys. Chem. B* 108, 1677 (**2004**).
24. X. P. Cao and R. J. Hamers, *J. Phys. Chem. B* 106, 1840 (**2002**).
25. E. K. Hlil, L. Kubler, J. L. Bischoff, and D. Bolmont, *Phys. Rev. B* 35, 5913 (**1987**).
26. X. Cao and R. J. Hamers, *J. Vac. Sci. Technol. B* 20, 4 (**2002**).
27. X. Cao and R. J. Hamers, *J. Am. Chem. Soc.* 123, 10988 (**2001**).
28. Th. Kugler, U. Thibaut, M. Abraham, and G. Folkers, and W. Göpel, *Surf. Sci.* 260, 64 (**1992**).
29. C. Shannon and A. Campion, *Surf. Sci.* 227, 219 (**1990**).
30. J. Eng, Jr., K. Raghavachari, L. M. Struck, Y. J. Chabal, B. E. Bent, G. W. Flynn, S. B. Christman, E. E. Chaban, G. P. Williams, K. Radermacher, and S. Mantl, *J. Chem. Phys.* 106, 9889 (**1997**).
31. J. Kim, K. Kim, and K. Yong, *J. Vac. Sci. Technol. A* 20, 1582 (**2002**).
32. J. W. Kim, M. Carbone, M. Tallarida, J. H. Dil, K. Horn, M. P. Casaletto, R. Flammini, and M. N. Piancastelli, *Surf. Sci.* 559, 179 (**2004**).
33. M. P. Casaletto, R. Zanoni, M. Carbone, M. N. Piancastelli, L. Aballe, K. Weiss, and K. Horn, *Surf. Sci.* 505, 251 (**2002**).
34. Y. Bu and M. C. Lin, *Langmuir* 10, 3621 (**1994**).
35. X. J. Zhou, Q. Li, and K. T. Leung, *J. Phys. Chem. B* 110, 5602 (**2006**).
36. W. Kern and D. A. Puotinen, *RCA Rev.* 31, 187 (**1970**).
37. Q. Li and K. T. Leung, *Surf. Sci.* 479, 69 (**2001**).
38. C. C. Cheng and J. T. Yates, Jr., *Phys. Rev. B* 43, 4041 (**1991**).
39. W. Kohn and L. J. Sham, *Phys. Rev.* 140, A1133 (**1965**).
40. M. J. Frisch, G. W. Trucks, H. B. Schlegel, G. E. Scuseria, M. A. Robb, J. R. Cheeseman, J. A. Montgomery, Jr., T. Vreven, K. N. Kudin, J. C. Burant, J. M. Millam, S. S. Iyengar, J. Tomasi, V. Barone, B. Mennucci, M. Cossi, G. Scalmani, N. Rega, G. A. Petersson, H. Nakatsuji, M. Hada, M. Ehara, K. Toyota, R. Fukuda, J. Hasegawa, M. Ishida, T. Nakajima, Y. Honda, O. Kitao, H. Nakai, M. Klene, X. Li, J. E. Knox, H. P. Hratchian, J. B. Cross, V. Bakken, C. Adamo, J. Jaramillo, R. Gomperts, R. E. Stratmann, O. Yazyev, A. J. Austin, R. Cammi, C. Pomelli, J. W. Ochterski, P. Y. Ayala, K. Morokuma, G. A. Voth, P. Salvador, J. J. Dannenberg, V. G. Zakrzewski, S. Dapprich, A. D. Daniels, M. C. Strain, O. Farkas, D. K. Malick, A. D. Rabuck, K. Raghavachari, J. B. Foresman, J. V. Ortiz, Q. Cui, A. G. Baboul, S. Clifford, J. Cioslowski, B. B. Stefanov, G. Liu, A. Liashenko, P. Piskorz, I. Komaromi, R. L. Martin, D. J. Fox, T. Keith, M. A. Al-Laham, C. Y. Peng, A. Nanayakkara, M. Challacombe, P. M. W. Gill, B. Johnson, W. Chen, M. W. Wong, C. Gonzalez, and J. A. Pople, Gaussian 03, Gaussian, Inc., Wallingford, CT (**2005**).
41. A. D. Becke, *J. Chem. Phys.* 98, 5648 (**1993**).
42. C. Lee, W. Yang, and R. G. Parr, *Phys. Rev. B* 37, 785 (**1988**).
43. X. Lu, X. Xu, N. Wang, Q. Zhang, and M. C. Lin, *J. Phys. Chem. B* 105, 10069 (**2001**).
44. C. Mui, M. A. Filler, S. F. Bent, and C. B. Musgrave, *J. Phys. Chem. B* 107, 12256 (**2003**).
45. A. Radi, M.Sc. Thesis, University of Waterloo, Waterloo, Canada (**2009**).
46. R. E. Penn and R. F. J. Curl, *Chem. Phys.* 55, 651 (**1971**).
47. R. E. Penn and R. J. J. Olsen, *Mol. Spectrosc.* 62, 423 (**1976**).
48. S. Leavell, J. Steichen, and J. L. J. Franklin, *Chem. Phys.* 59, 4343 (**1973**).
49. I. Vorobyov, M. C. Yappert, and D. B. DuPre, *J. Phys. Chem. A* 106, 668 (**2002**).
50. B. Miller, Advanced Organic Chemistry: Reactions and Mechanisms, Prentice-Hall, New Jersey (**1998**).
51. L. Zhang, A. Chatterjee, M. Ebrahimi, and K. T. Leung, *J. Chem. Phys.* 130, 121103 (**2009**).
52. J. L. Armstrong, J. M. White, and M. Langell, *J. Vac. Sci. Technol. A* 16, 123 (**1997**).
53. Y.-R. Luo, Bond Dissociation Energies, CRC Handbook of Chemistry and Physics, edited by D. R. Lide, 88th edn., CRC Press/Taylor and Francis, Boca Raton (**2008**).
54. H. Liu and R. J. Hamers, *Surf. Sci.* 416, 354 (**1998**).
55. J. S. Hovis and R. J. Hamers, *J. Phys. Chem. B* 101, 9581 (**1997**).
56. M. Ebrahimi, J. F. Rios, and K. T. Leung, *J. Phys. Chem. C* 113, 281 (**2009**).

Received: 8 February 2011. Revised/Accepted: 2 May 2011.